



CFD Simulation of Air-Glass Beads Fluidized Bed Hydrodynamics

S. Aboudaoud[†], S. Touzani, S. Abderafi and A. Cheddadi

*Research team, Modeling of Energy Systems, Mechanical Materials and Structures, and Industrial Processes (MOSEM2PI),
Mohammadia School of Engineers, Mohammed V University in Rabat, P. O. Box 765 Agdal, Rabat, Morocco*

[†]Corresponding Author Email: souadaboudaoud@research.emi.ac.ma

ABSTRACT

The hydrodynamic behaviour of air-glass beads bubbling fluidized bed reactor containing spherical glass beads is numerically studied, using OpenFoam v7 CFD software. Both Gidaspow and Syamlal-O'Brien drag models are used to calculate momentum exchange coefficients. Simulation predictions of pressure loss, bed expansion rate, and air volume fraction parameters were compared and validated using data, existing in the literature obtained experimentally and performed by other numerical softwares. Pressure loss and rate of bed expansion were calculated with relative root mean square error (RMSE) equal to 0.65 and 0.095 respectively; Syamlal-O'Brien model is considered more accurate than Gidaspow model. Hence, numerical model reliability developed on OpenFoam was also proved. The hydrodynamic aspect study of the fluidized bed reactor was then performed, to analyse the impact of inlet air velocity (U) on particles motion. It was revealed that with U increment, air and glass beads axial velocities increase in the reactor centre and decrease in the sidewalls. Thus, a greater particle bed expansion is induced and the solid particles accumulated highly on the reactor sidewalls. In general, with the increase of U , the solid volume fraction decreases from 0.63 to 0.58 observed at 0.065 m/s and 0.51 m/s, respectively.

Article History

Received January 4, 2023

Revised April 21, 2023

Accepted April 24, 2023

Available online July 1, 2023

Keywords:

CFD modelling

Eulerian-Eulerian approach

Fluidized bed reactor

Hydrodynamic

Multiphase flow

OpenFoam.

1. INTRODUCTION

Morocco has a significant potential for combustible municipal waste that can be exploited for the production of biofuels (Aboudaoud et al. 2022; El Kourdi et al., 2022). Fluidized bed has been found to be an efficient and interesting solution for municipal solid waste valorization in bioenergy, by comparison to the various pyrolysis technologies (El Kourdi et al., 2023). It is also an economical technology performing thermochemical processes in general (Yates & Lettieri, 2016). In thermochemical conversion processes, efficiency is mainly related to chemical reactions and heat transfer and gas-solid mixing, which have a great importance in mass and energy transfer (Philippsen et al., 2015). The fluidized bed consists of fine inert particles, including sand, alumina, limestone, and dolomite for tar reforming. The most used is sand, with an average diameter of about 1 mm, allowing to reach fluidization speeds of 1-3 m/s (Materazzi & Lettieri, 2017). Fluidized bed technology faces several challenges, including ash agglomeration, low carbon conversion, and hydrodynamic complexity. However, understanding hydrodynamic aspect of solid-gas flow, fluidization behaviour, and fluidizing gas interaction with particles bed are preliminary for

maintaining good operation and controlling fluidization parameters (Di Renzo et al., 2021).

Experimental works using fluidized bed systems with many interdependent conditions are quite tedious and costly in time and money. Thanks to the advanced development of computational fluid dynamics (CFD) modelling, multiphase systems such as fluidized beds can be modelled and simulated allowing to study them and understand the general physics controlling their performance. Mainly, two approaches have been adopted for modelling multiphase flows in such technologies: discrete and continuous. The first one is based on Lagrangian model (Fatti & Fois 2021), considering the particle bed behaviour as the sum of the behaviours of each particle. Newtonian equations are solved to describe each particle's motion, including inter-particles collisions effects as well as the gas forces exerted on them. Although the discrete method gives accurate results, it is only valid for dilute multiphase flows containing small solid volume fraction (Stanly et al., 2017). Moreover, this approach is very expensive in terms of numerical calculations. Concerning the continuous approach, it is based on Eulerian model. The different fluid-solid phases are considered as interpenetrated and continuous. This

Nomenclature			
C_D	drag coefficient	\vec{U}	velocity
Co	co-number	y	height coordinate measured from distributor
C	particle fluctuating velocity	α	volume fraction, dimensionless
d	particle diameter	β	heat transfer coefficient
e	internal energy	β_{g-s}	gas/ solid momentum exchange coefficient
e_{ss}	restitution coefficient	γ_i	thermal diffusivity
\vec{g}	acceleration due to gravity	$\gamma\theta_s$	dissipation term for inelastic collisions
$g_{0,ss}$	radial distribution coefficient	ε_i	voidage
h_i	enthalpy	μ	dynamic viscosity
H	bed height	θ_i	granular temperature
H_0	static bed height	$\lambda\theta_s$	apparent viscosity
\bar{T}	stress tensor, dimensionless	μ_s	shear viscosity
I_{2D}	second invariant of the deviatoric stress tensor	κ_{θ_s}	granular energy conductivity
K	kinetic energy	ρ	density
p	pressure	$\bar{\tau}$	viscous stress tensor
ΔP	pressure drop	Φ_s	degree sphericity
$p_{s,fr}$	frictional pressure	Subscripts	
Re_s	relative Reynolds number	g	gas
RMSE	Root Mean Square Error	i	general index
t	time	mf	minimum fluidization
T	temperature	p	particle
U	superficial gas velocity	s	solid

approach is often coupled with kinetic granular flow theory (KTGF), which considers grains in a state of continuous agitation in the fluid and is used to determine the solid phase viscous stress term, based on the shear and apparent viscosities as well as the solids pressure calculation (Chen et al., 2019). Gas-solid interphase momentum exchange is expressed using the drag force. Choosing an adequate drag model is essential for accurate modelling, being one of the main parameters influencing hydrodynamic behaviour (Pei et al., 2012). Different drag models are available in the literature and the most frequently used as stated by Ullah et al. (2019): Syamlal O'Brien Gidaspow, and Wen-Yu.

Using continuous Eulerian approach, several authors have been interested in simulating hydrodynamics behaviour of different inert bed materials in fluidized bed. Diverse softwares were employed and various drag models were compared, to predict pressure loss, bed extension, and time-averaged solid fraction curves. Taghipour et al. (2005) have studied experimentally and numerically glass beads- air flow in a 2D fluidized reactor, employing Ansys-Fluent 6.0 CFD software. For the momentum exchange coefficient calculations, the three drag models mentioned above were applied. Those models gave quite similar results. In comparison with the data from the experiment, bed expansion predictions were in good agreement as well as for the pressure-drop values, but only at higher superficial gas velocities. Sahoo and Sahoo. (2014) found that Gidaspow model shows good results between Ansys-Fluent 13.0 simulation and experimental measurements for Geldart-A class red mud particles. Venier et al. (2019) have predicted fluidization curves, bubble size and solid volume fraction for particles

type: Geldart-A (Cristabolite sand), Geldart-B (sand) and Geldart-D (Urea). Taking into account particle sphericity in Gidaspow drag model, both Ansys-Fluent v19.2 and OpenFoam v6.0 softwares provided good bubble and solid fractions simulations, but Ansys-Fluent was found to be less accurate for bubble size forecast. Bhusare et al. (2017) found that OpenFOAM v2.3.1 simulations of two-phase bubble columns are quietly similar to experimental data and Ansys-Fluent calculations. Herzog et al. (2012) have tested three software packages: Ansys-Fluent v 6.3, MFIX and OpenFoam v2.0, on simulating hydrodynamic aspect of Geldart-B glass beads, using Gidaspow and Syamlal-O'Brien models. OpenFoam was not retained, because numerical results were inconsistent with experimental study. By contrast, the other two software packages gave better results, especially in bubbling regime, for both drag models. Cardoso et al. (2018) have improved Syamlal-O'Brien model performance by modifying it to compute biomass fluidisation, using Ansys-Fluent 15. Chauhan et al. (2022) have compared drag models performances on Geldart-D class coal ash fluidization properties, employing Ansys-Fluent software v14.0. Gidaspow model was found to be unable to predict coal ash fluidization, contrarily to Syamlal O'Brien model. Kia and Aminian (2017) have reported that Gidaspow model is suitable for pressure loss prediction during fixed bed regime for glass beads, red mud and quartz sand particles. For dilute flow regimes, Syamlal-O'Brien model is most adequate. Liu and Hinrichsen (2014) have carried out simulation by OpenFoam v2.1.1 of two fluidized beds containing glass beads particles with different gas suppliers. Syamlal-O'Brien model has simulated successfully beds with uniform gas supply, while Gidaspow model has been more suitable to compute beds with gas introduction in the

centre. Shi et al. (2019) have highlighted the impact of Ansys-Fluent 16.2 turbulence model choice on Geldart-B class particles fluidisation simulation. RANS model associated to Syamlal-O'Brien model is much suitable than RANS or Laminar models with Gidaspow model.

Bibliographic synthesis shows that for various bed material types, Syamlal-O'Brien and Gidaspow models are mostly used to describe hydrodynamic fluidization behaviour. Their accuracy varied in a case study to another. Additionally, few authors have given details on glass beads particles motion during bubbling fluidization regime. According to Herzog et al. (2012), OpenFoam software offers the worst result compared to Ansys-Fluent and MFIX softwares and needs further improvement. In this work, our objective is to improve the performance of the Eulerian numerical model, using OpenFoam v7 and study both air and glass beads movement in bubbling fluidized reactor. First, the numerical model developed on OpenFoam will be validated basing on the literature, by studying Syamlal-O'Brien and Gidaspow models impact on pressure loss, bed expansion ratio and glass beads volume fraction. Then, the most adequate drag model will be chosen to describe air-glass beads fluidization motion. Afterwards, examining the gas superficial velocities influence on the glass beads particles movement will be carried out in the bubbling regime, which has not been studied, so far as we know.

2. MATHEMATICAL MODEL

The simulation of the fluidized bed consists in using a two-fluid Eulerian model composed of mass, momentum, and energy conservation equations for each phase: gas (air) and solid (glass beads). The solid particle fluctuation energy conservation equation derived from the granular flow kinetic theory (KTGF) is also employed to determine the stress terms in solid phase momentum equation (Taghipour et al., 2005). The fundamental equations are presented below, for developing the fluidized bed reactor simulation model.

2.1 Model's Equations

The governing equations were determined for air and glass beads. Equation (1) and Equation (2) represent mass conservation for the two studied phases, gas (g) and solid (s), given respectively by:

$$\frac{\partial}{\partial t}(\alpha_g \rho_g) + \nabla \cdot (\alpha_g \rho_g \vec{U}_g) = 0 \quad (1)$$

$$\frac{\partial}{\partial t}(\alpha_s \rho_s) + \nabla \cdot (\alpha_s \rho_s \vec{U}_s) = 0 \quad (2)$$

Where: α_i is volume fraction, ρ_i is density and \vec{U}_i is velocity, with index $i=g$, for the gas phase and $i=s$, for the solid phase. For each cell, the sum of gas and solid phases volume fractions is equal to unity:

$$\alpha_g + \alpha_s = 1 \quad (3)$$

Equations (4) and (5) give the momentum conservation for both phases.

$$\begin{aligned} \frac{\partial}{\partial t}(\alpha_g \rho_g \vec{U}_g) + \nabla \cdot (\alpha_g \rho_g \vec{U}_g \vec{U}_g) = \nabla \cdot \vec{\tau}_g \\ - \alpha_g \nabla p + \sum \beta_{g-s} (\vec{U}_g - \vec{U}_s) + \alpha_g \rho_g \vec{g} \end{aligned} \quad (4)$$

$$\begin{aligned} \frac{\partial}{\partial t}(\alpha_s \rho_s \vec{U}_s) + \nabla \cdot (\alpha_s \rho_s \vec{U}_s \vec{U}_s) = \nabla \cdot \vec{\tau}_s \\ - \alpha_s \nabla p - \nabla p_s + \sum \beta_{g-s} (\vec{U}_g - \vec{U}_s) + \alpha_s \rho_s \vec{g} \end{aligned} \quad (5)$$

Where, p is gas pressure and \vec{g} is gravitational acceleration.

The coupling of the two phases occurs through the air-glass beads momentum exchange coefficient, β_{g-s} , that varies with the type of drag model. Syamlal-O'Brien and Gidaspow models have been selected (Eq. (A1) and Eq. (A2) in Table A1, Appendix). Those models have been proved to be reliable for fluidized beds hydrodynamics simulations, with very fine meshing (Ullah et al., 2013). The viscous stress tensors, for air (τ_g) and glass beads (τ_s) phases, are expressed in equations (A3) and (A4), respectively. In the solid phase viscous stress expression, μ_s , λ_s , and p_s express dynamic viscosity, apparent viscosity, and granular pressure, respectively. These three properties were determined by granular flow kinetic theory (KTGF).

Energy equations (Eq. (6) and Eq. (7)) for both phases are given below, respectively:

$$\begin{aligned} \frac{\partial}{\partial t}(\alpha_g \rho_g (e_g + K_g)) + \nabla \cdot (\alpha_g \rho_g (e_g + K_g) \vec{U}_g) = \\ - \left(\frac{\partial \alpha_g}{\partial t} p + \nabla \cdot (\alpha_g \vec{U}_g p) \right) + \nabla \cdot (\alpha_g \gamma_g (\nabla h_g)) + \beta \Delta T \end{aligned} \quad (6)$$

$$\begin{aligned} \frac{\partial}{\partial t}(\alpha_s \rho_s (e_s + K_s)) + \nabla \cdot (\alpha_s \rho_s (e_s + K_s) \vec{U}_s) = \\ - \left(\frac{\partial \alpha_s}{\partial t} p + \nabla \cdot (\alpha_s \vec{U}_s p) \right) + \nabla \cdot (\alpha_s \gamma_s (\nabla h_s)) + \beta \Delta T \end{aligned} \quad (7)$$

Where: e_i , K_i , h_i , γ_i , β and T are the internal energy, kinetic energy, enthalpy, thermal diffusivity, heat transfer coefficient and temperature, respectively.

2.2 Granular Flow Kinetic Theory

Solids in Eulerian approach are modelled as fluid; thus, it is imperative to introduce equations corresponding to particle's rheology. This model is expressed as additional source terms embedded in the solid's viscous stress, τ_s , presupposing the inelastic nature of collisions (Fatti & Fois 2021). Since the solid phase stress varies with fluctuations in particle velocity, a granular energy equilibrium equation associated with these fluctuations is introduced into the model to complement the equations described in section 2.1 for both studied phases (Ngo et al., 2013).

KTGF theory permits the calculation of solid pressure, p_s , solid shear and apparent viscosities, μ_s and λ_s related to "granular temperature" defined by: $\Theta=c^2/3$, with 'c' is particles fluctuation velocity (Santos et al., 2013).

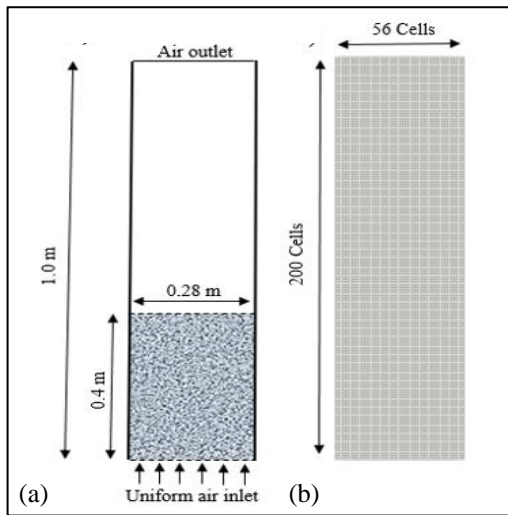


Fig. 1. a) Scheme of fluidized bed reactor with the glass beads. b) Mesh structure with the number of cells in x and y direction.

Granular temperature expresses the macroscopic kinetic energy of random particles motion and replaces thermodynamic temperature in solid phase treatment. Once this quantity is determined, it is possible to involve an equation that describes KTGF; it is the kinetic energy equation of fluctuation, which considers particles fluctuation energy conservation reported in equation (8) (Liu & Hinrichsen, 2014):

$$\frac{3}{2} \cdot \left[\frac{\partial}{\partial t} (\rho_s \alpha_s \Theta_s + \nabla \cdot (\rho_s \alpha_s \bar{U}_s \Theta_s)) \right] = (-p_s \bar{I} + \bar{\tau}) : \nabla \bar{U}_s + \nabla \cdot (\kappa_{\Theta_s} \nabla \Theta_s) - \gamma_{\Theta_s} \quad (8)$$

The constituent equations needed to complete the model are grouped in Table A1 (Appendix). Inter-particles collisions have lower importance for dense flows with low-shear and high particles volume fraction, while frictional stresses are significant. In this study, particles volume fraction is higher than the critical value, set at $\alpha_{s,min} = 0.5$, and it approaches packing limit max, 0.63. Thus, the frictional stress joins the stress provided in the kinetic theory ($\tau_s = \tau_{s,kt} + \tau_{s,f}$). Hence, the frictional viscosity appears in the shear viscosity (Eq. A5) and defined according to the Schaffer model in Eq. (A9) (Appendix).

3. METHODOLOGY AND PROCEDURE

CFD model reliability described above was tested by simulating air-glass beads fluidization, utilizing OpenFoam. Obtained results accuracy was based on Taghipour et al. (2005) experiment study. This section presents the studied system and the followed simulation procedure.

3.1 Studied System

As already mentioned by Taghipour et al. (2005), fluidized beds hydrodynamic studies are often simulated in 2D, to provide a good visualization of fluidization characteristics, that cannot be seen in 3D. Therefore, our CFD model is computed in 2D. Figure 1 shows the studied system dimensions and geometry.

Table 1 Parameters and operating conditions of the fluidized bed simulation.

Parameter	Value
<i>Solid phase (Glass Beads)</i>	
Bed height (m)	1.0
Bed width (m)	0.28
Static bed height (m)	0.4
Particle diameter (m)	275×10^{-6}
Particle density (kg/m ³)	2500
Restitution coefficient, e_{ss}	0.9
Packed bed fraction	0.6
Packed bed max fraction	0.63
Wall/particle specularity coefficient	0.2
Minimum fluidization velocity U_{mf} (m/s)	0.065
<i>Gas phase (Air)</i>	
Density (kg/m ³)	1.225
Viscosity (kg/(m.s))	1.82×10^{-5}
Prandtl number	0.7
Inlet temperature (K)	288

Computational study parameters presented in Table 1 as well as boundary conditions, are similar to experimental conditions taken into account by Taghipour et al. (2005). At reactor bottom, particles cannot pass through the inlet ports. So, glass beads velocity was fixed at zero, as initial condition. An “interstitial inlet velocity” boundary condition is applied, which determines the superficial air velocity. For all sidewalls, no-slip condition is assumed for air, setting air velocity at walls to zero. In a granular flow, the particles do not stick to the walls (no-slip condition) and do not slide freely on the wall (slip condition); they behave between these two conditions. Therefore, the “Johnson & Jackson” condition was proposed as a boundary condition at the walls for glass beads velocity, as well as for granular temperature (Johnson & Jackson, 1987). For air and glass beads temperature fields, initial and inlet temperature is 288K, while "zeroGradient" and "inletOutlet" conditions are considered at walls and outlet, respectively.

3.2 CFD Simulation Procedure

CFD simulation was performed using OpenFoam v7 software by choosing a solver named twoPhaseEulerFoam. The unsteady mass and momentum and energy conservation equations were solved with PIMPLE algorithm which is a PISO/SIMPLE algorithms combination. General CFD simulation algorithm for the twoPhaseEulerFoam solver is shown in Fig. 2 A computer with the following specifications was employed to run simulations: Professional Windows 10, 64-bit operating system, with 8.00 Go RAM, and intel® Core™ i7-6700 CPU processor at 3.40GHz.

A mesh study is conducted using a 2-D mesh with different grid resolutions and different time steps: three mesh grids for two-time steps set to 2×10^{-4} s and 5×10^{-4} s, respectively. Using Syamlal-O’Brien model, pressure loss for five superficial air velocities (0.03 m/s, 0.065 m/s, 0.26

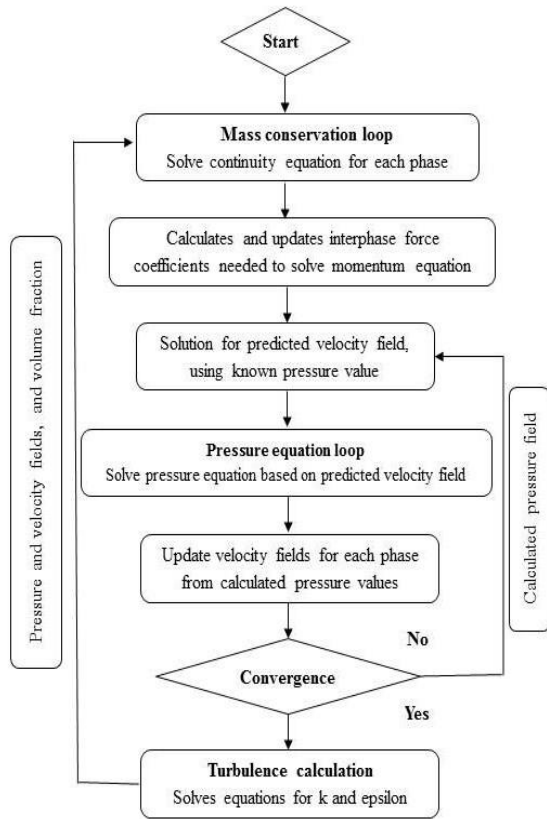


Fig. 2. PIMPLE algorithm to solve two Phase EulerFoam solver (Bhusare et al., 2017).

m/s, 0.38 m/s, and 0.51 m/s) is computed for the six mesh grids with a Co-number of 0.4 (Fig. 3). The Courant number is used to define the time step necessary to obtain numerical stability and temporal precision. It is expressed by:

$$Co = (\delta t \cdot |U|) / \delta x \quad (9)$$

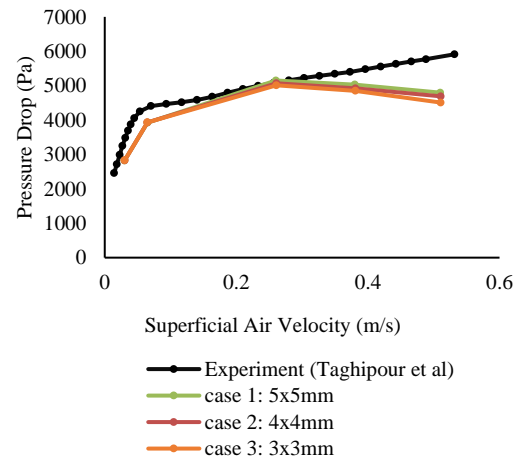
In which: δt , $|U|$, and δx represent time step, velocity magnitude and cell size, respectively. Therefore, a Courant number less than 1 is desired (Liu & Hinrichsen, 2014).

The results of each one of the six grids are compared to Taghipour et al. (2005) experiment, by calculating relative mean square error (RMSE) based on the pressure drop curves (Table 2). The RMSE obtained with a time step of 2×10^{-4} s is the lowest for all studied grids compared to 5×10^{-4} s. In order to reduce computational costs, the mesh representing less error and less execution time is 5x5 mm grid size with 2×10^{-4} s time step. Thus, this mesh is considered for further simulations.

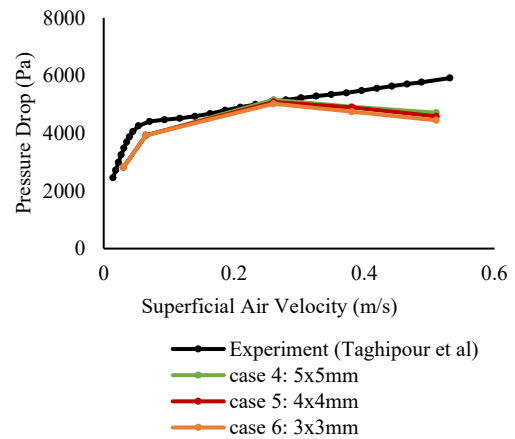
Table 2 Mesh study of six cases, with three different grid sizes and two different time steps.

Grid size (mm)	Cells (x direction)	Cells (y direction)	Time step: 2×10^{-4} s		Time step: 5×10^{-4} s	
			Exec time (s)	RMSE	Exec time (s)	RMSE
5x5	56	200	24616	0.6	10690	0.66
4x4	70	250	19417	0.66	56717	0.7
3x3	93	333	37901	0.74	90348	0.78

The pressure drop variation curve versus superficial air velocity shows a significant deviation between the calculated and experimental values for high gas velocities equal to 0.38 m/s and 0.51 m/s (Fig.3). The relative difference defined as the absolute discrepancy between measured and calculated values divided by measured one, was calculated. It is varying between 8% and 18% found for the superficial gas velocity 0.38 m/s and 0.51 m/s, respectively. The reason behind this significant difference will be detailed in the next section below.



(a) Time step = 2×10^{-4} s



(b) Time step = 5×10^{-4} s

Fig. 3. Comparison of experimental and calculated pressure drop values using Syamlal O'Brien drag model, for three sets of grids with two different time steps set to (a) 2×10^{-4} s and (b) 5×10^{-4} s.

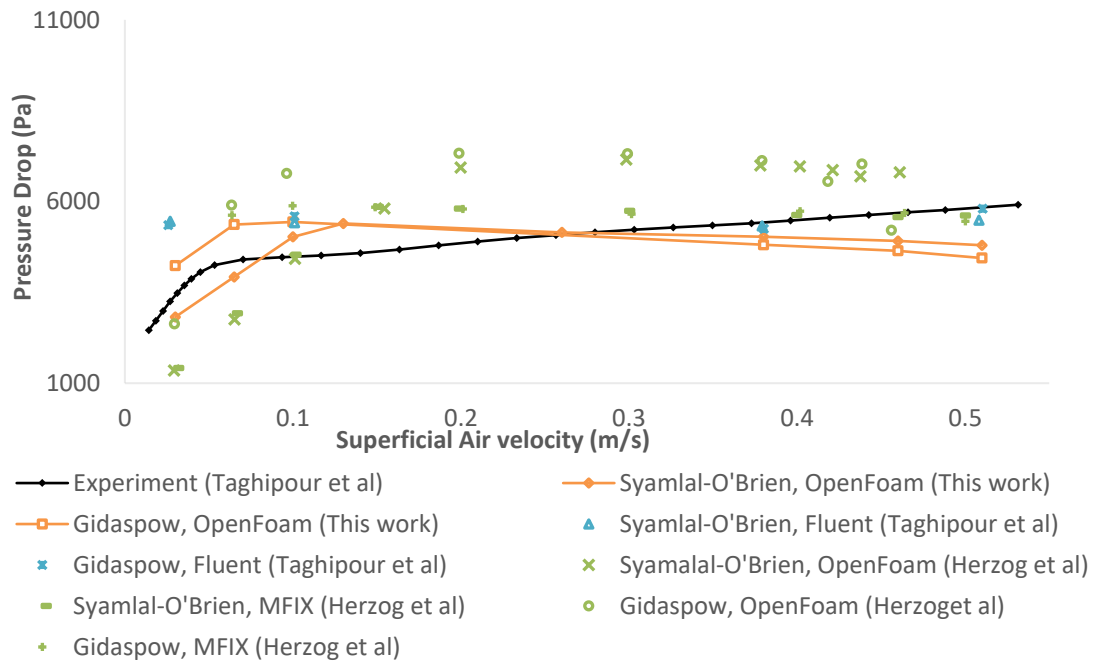


Fig. 4. Comparison of experimental and calculated pressure drop values, using Syamlal-O'Brien and Gidaspow drag models.

4. RESULTS AND DISCUSSION

Pressure drop, particle bed expansion rate, and average air volume fraction were calculated, using Syamlal-O'Brien and Gidaspow models. A comparison with obtained results and those of literature is made with the aim of validating the current CFD model. Then, this latter was used to study the fluidized bed dynamic behaviour and properties. This study was limited to the bed functioning in the bubbling fluidization regime. According to Geldart classification, particles used belong to Geldart-B class, whereby the minimum fluidization and bubbling velocities, U_{mf} and U_{mb} are confounded, equal to 0.065m/s.

4.1 CFD Model Validation

According to simulation findings, the steady state was obtained after flow time of 3s. CFD simulations were conducted to determine pressure loss ΔP , measured from $y=0.03$ m to $y=0.6$ m and bed expansion ratio H/H_0 , for inlet air velocities, varying between 0.03 m/s and 0.51 m/s corresponding to $0.5 U_{mf}$ and $7.8 U_{mf}$, respectively; characterizing the two hydrodynamic regimes of the fixed and bubbling bed.

4.1.1 Pressure Drop

In this work, pressure loss within the reactor was calculated for various inlet air velocities, using Gidaspow and Syamlal-O'Brien models. In Fig. 4, the obtained values were compared to Taghipour et al. 2005 experiment results and also with numerical data obtained using OpenFoam, Ansys-fluent, and MFIX softwares (Taghipour et al., 2005; Herzog et al., 2012). In general, pressure drop values calculated using Ansys-Fluent and MFIX softwares are in close accordance with experimental results when superficial air velocity is high.

However, our results using OpenFoam software are more consistent with experimental findings for low inlet air velocities (0.03 m/s to 0.26 m/s), than those obtained for high velocities (0.38 m/s to 0.51 m/s). Similarly to (Taghipour et al., 2005) and (Herzog et al., 2012), for $U > U_{mf}$, the pressure drop values have the same tendency different to the experimental results which are increasing. According to Bounaceur (2009), the numerical results are theoretically reasonable. Indeed, for low inlet gas velocity during fixed bed regime, pressure loss increases because of fluid friction on particles and walls surfaces. In the bubbling fluidization regime ($U > U_{mf}$), when the particles are fluidized, the bubbles appear which separate the solid particles and increase the fluid cross-sectional area, resulting to decrease the particles frictions. Therefore, the pressure drop becomes independent to the gas velocity and remains constant. This constant pressure is equivalent to the apparent weight of the particles per the bed surface unit. Regarding the deviated results obtained experimentally, they are probably attributed to the measurement methods or to the nature of the gas distributor used. Another important point that was mentioned by (Taghipour et al., 2005) is that he used a perforated plate to distribute the gas in the inlet of his experiment, which is not taken into account in CFD models. This could have led to increase the bubble size and number resulting a high pressure drop.

Despite the fact that the three codes use finite volume method (FVM) and Eulerian-Eulerian approach to treat the mathematical model with the same boundary and operating conditions, the obtained results are slightly different. It can be related to the numerical resolution method of Navier-Stockes equations with the problem of pressure-velocity coupling. Ansys-Fluent and MFIX both utilise the Semi-Implicit Method for Pressure-Linked

Table 3 RMSE calculation of pressure drop for different numerical studies.

Numerical tool	Syamal-O'Brien	Gidaspow	Reference
OpenFoam	0.65	1.00	This work
OpenFoam	1.53	1.58	Herzog et al. (2012)
MFIX	0.95	0.94	Herzog et al. (2012)
Ansys-Fluent	1.23	1.23	Taghipour et al. (2005)

Equations algorithm (SIMPLE), which gives more stable solutions but very slow and commonly used in stationary cases. While, the numerical solution of the model, developed in OpenFoam, revolve on PIMPLE algorithm which combines two algorithms SIMPLE and PISO (Pressure Implicit with Splitting of Operator). It is a hybrid system used in transient cases, given both fast and stable solutions. Another reason can be attributed to the choice of the turbulence model that the other numerical works did not evoke. Indeed, [Shi et al. \(2019\)](#) have shown that turbulence and drag models combination can impact the simulation accuracy.

Moreover, [Herzog et al. \(2012\)](#) also used the same software "OpenFoam", but found very large deviation with experiment results during the whole calculations, quantified by high RMSE of 1.53 and 1.58, using Syamlal-O'Brien and Gidaspow models, respectively. In our work, this discrepancy was reduced, by adjusting the numerical convergence parameters, which control the convergence, the stability and the accuracy of the discretized equation solutions of pressure, velocity and solid and gas phase fractions. A 3nOuterCorrectors was fixed for the external loop constituting the SIMPLE correctors, solving the momentum equation, to improve the stability of second order time discretization schemes. Meanwhile, to solve the Poisson and continuity equations, 1nCorrector was sufficient for the internal loop constituting the PISO correctors to enhance both accuracy and stability. A relaxation factor of 1 was chosen to accelerate the algorithm convergence.

The model performance of the various numerical works was evaluated by calculating RMSE, for both drag models. Computational results are grouped in Table 3, where pressure loss prediction accuracy is analysed by calculating the RMSE error for this work and the previous studies existing in literature. The results provided by OpenFoam in this present study are presenting the lowest RMSE (0.65), compared to the other works which are ranging between 0.94 and 1.58. In our case, it is noticed that Syamlal-O'Brien model is more efficient for pressure drop curve prediction. Indeed, [Liu and Hinrichsen. \(2014\)](#) also found that Syamlal-O'Brien model is more suitable for simulating fluidized bed with uniform gas injection in dense or dilute flow regimes, while Gidaspow model was recommended only for beds with gas inlet in the centre. [Solli and Agu \(2017\)](#) adjusted Syamlal-O'Brien model with some parameters relative to U_{mf} measured experimentally, and found good simulation of bubbling bed behaviour. Actually, [Ullah et al. \(2019\)](#) described Syamlal-O'Brien model to be a generalized model and can be fitted according to minimum fluidization and

terminal velocities of the particles, whereas, Gidaspow model results from combining Wen-Yu and Ergun correlations. The first is applicable when internal forces are insignificant and viscous forces are dominant in the flow, while, the second relates the drag force to the pressure loss and it is more suitable only for a bed with high solid volume fraction. According to [Kia and Aminian \(2017\)](#), the Gidaspow model does not consider the drag coefficient, C_D , for low gas volume fractions $\alpha_g < 0.8$. In this work, $\alpha_g = 0.4$ signifying that drag coefficient has been disregarded for the two regimes: dense and dilute. Same results have been found by [Liu and Hinrichsen. \(2014\)](#) and [Chauhan et al. \(2022\)](#). In order to ameliorate the Gidaspow model prediction, [Venier et al. \(2019\)](#) suggested to take into account the sphericity factor which will improve the bubble formation.

4.1.2 Bed Height Expansion Ratio

Figure 5 shows comparison of time-averaged bed expansion rate predicted numerically using Syamlal-O'Brien and Gidaspow models with experiment results at different inlet air velocities. The curves relating to the numerical calculation show the same trend as the experimental curve; bed expansion ratio augments as inlet air velocity increases.

Compared to other softwares, using OpenFoam gives the lowest RMSE, which is around 0.095, by adopting Syamlal-O'Brien drag model (Table 4). The values calculated by Ansys-Fluent and MFIX are relatively similar with a RMSE of 0.12 and 0.116, respectively. However, by using Gidaspow model, the bed expansion ratio calculated with Ansys-Fluent and OpenFoam are quietly close with a small RMSE of 0.084 and 0.091, respectively. Therefore, using either OpenFoam or Ansys-Fluent softwares, Gidaspow model predicts a higher bed expansion at high superficial gas velocities. In fact, [Liu and Hinrichsen \(2014\)](#) affirmed that in a dilute flow regime ($U > U_{mf}$) and at high solid volume fractions ($\alpha_s > 0.2$), drag coefficient, C_D , is not considered in Gidaspow correlation (as mentioned previously). Thus, calculated air-glass beads momentum exchange coefficients, β_{g-s} become important than those computed with Syamlal-O'Brien model. This probably means that Gidaspow model neglects inter-particles cohesion impacts resulting from Van-der-Waals forces, as declared by [Taghipour et al. \(2005\)](#). Consequently, air-glass beads momentum exchange was over-estimated, rising air bubbles number and size became larger, leading to a high bed expansion and a low solid volume fraction. Hence, the Gidaspow drag model is suitable only for dense flow regime.

Table 4 RMSE calculation of bed height expansion ratio for various numerical studies

Numerical tool	Syamal-O'Brien	Gidaspow	Reference
OpenFoam	0.095	0.091	This work
OpenFoam	0.096	---	Herzog et al. (2012)
MFIX	0.116	---	Herzog et al. (2012)
Ansys-Fluent	0.120	0.084	Taghipour et al. (2005)

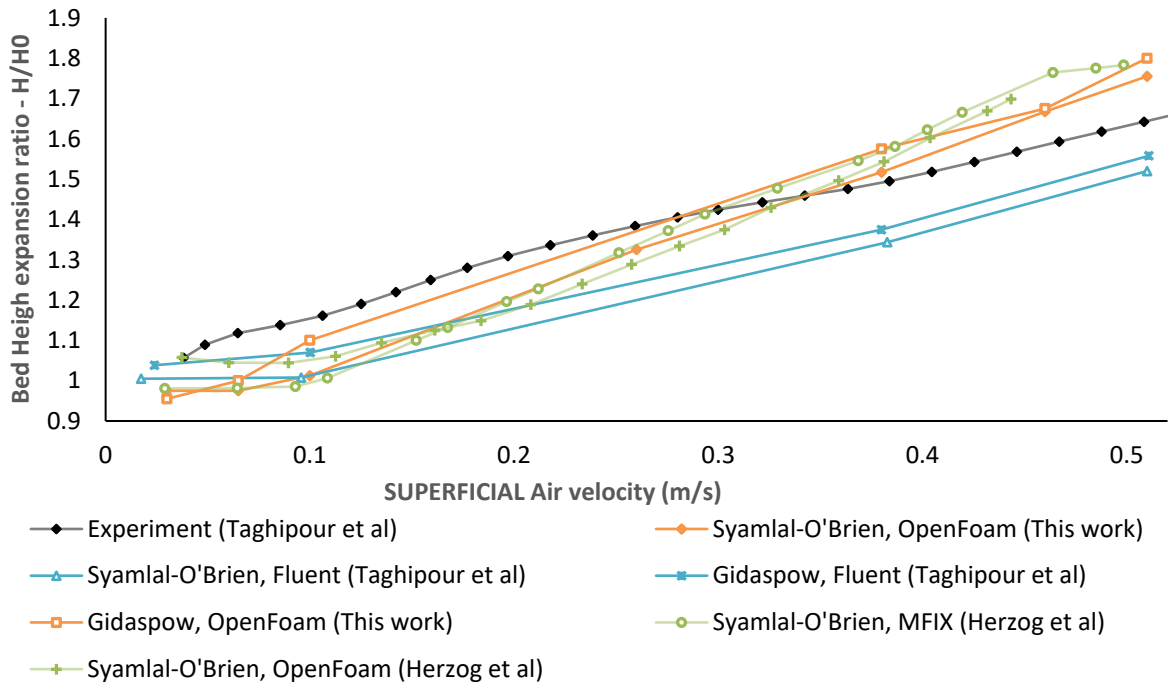


Fig. 5. Comparison of experimental and calculated bed height expansion ratio, using Syamlal-O'Brien and Gidaspow drag models.

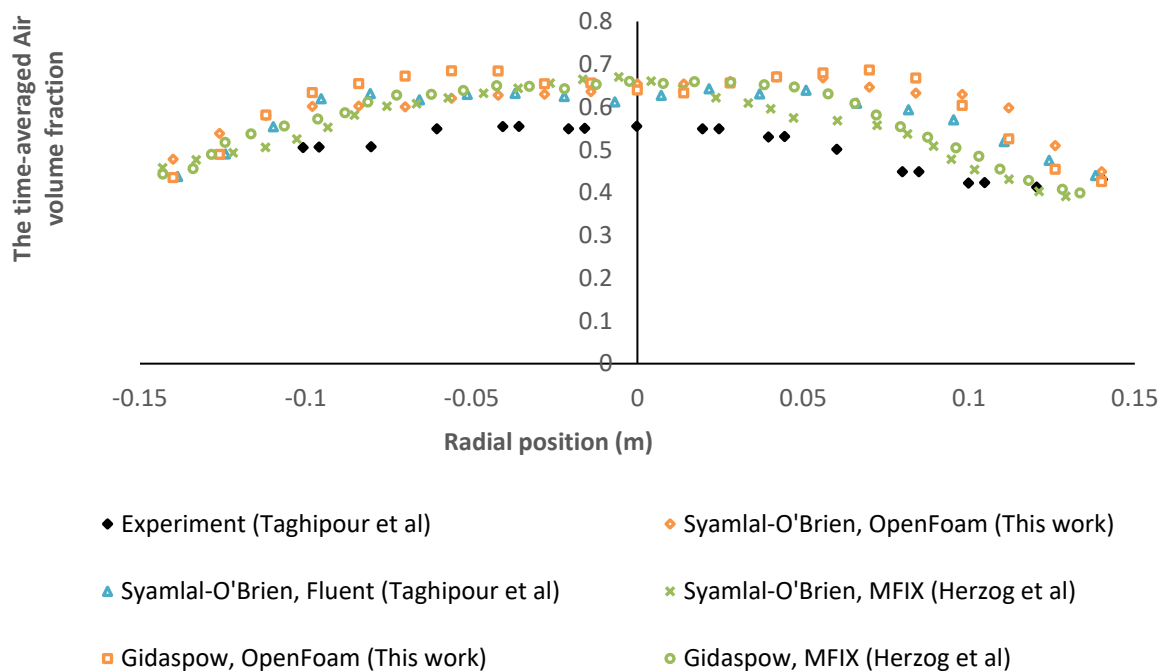


Fig. 6. Simulated and experimental time-averaged air volume fraction for superficial gas velocity $U = 0.46$ m/s at $y = 0.2$ m.

4.1.3 Time-Averaged Air Volume Fraction Profile

As shown on Fig. 6, simulation found results follow experiment data evolution and also those obtained by Ansys-Fluent (Taghipour et al., 2005), and MFIX (Herzog et al., 2012). Different computed profiles of air volume fraction represent a symmetrical pattern with good concordance at bed centre, where air volume fraction increases and reaches maximum values and decreases near

the walls. The discrepancy between computational and experiment results is quantified with RMSE calculation (Table 5). Applying Syamlal-O'Brien model, gave quite small RMSE values equal to 0.075, 0.098, and 0.122, using the three numerical tools MFIX, Ansys-Fluent, and OpenFOAM, respectively. However, even if the Gidaspow drag model yielded to the same symmetric evolution as obtained with Syamlal-O'Brien, the RMSE

Table 5 RMSE calculation of time-averaged gas volume fraction for various numerical studies

Numerical tool	Syamal-O'Brien	Gidasporw	Reference
OpenFoam	0.122	0.135	This work
MFIX	0.075	0.104	Herzog et al. (2012)
Ansys-Fluent	0.098	---	Taghipour et al. (2005)

values are slightly higher with 0.104 and 0.135 for MFIX and OpenFoam, respectively. In both numerical results and experimental data, the gas volume fraction is moderately low near the walls, while it is maximum in the bed centre. The reason behind this is the de-fluidization phenomenon of solid particles near the walls, showing the maximum solids. A maximum gas fraction is also observed due to fluidization occurring in the middle along the bed. A similar finding was also observed by Taghipour et al. (2005) in his simulation.

As summary, comparing numerical and experiment calculations (pressure loss, bed expansion ratio, and air volume fraction distribution), employing different simulators (OpenFoam, MFIX, and Fluent) and using particularly Syamlal O'Brien model, proved that our numerical model developed with OpenFoam is reliable and accurate. In the following section, the description of glass beads hydrodynamic aspect in a fluidized bed reactor is discussed.

4.2 Air - Glass Beads Fluidized Bed Hydrodynamic:

From the section above, Syamlal-O'Brien model proved to be the appropriate one to use. Therefore, it will be adopted to describe the impact of inlet air velocity. This latter has great influence on fluidization process, and consequently impacts air-glass beads hydrodynamic behaviour inside the reactor. Figure 7 shows the effect of

superficial air velocities on glass beads average volume fraction over the time 3-12 s for different superficial air velocities (0.065 m/s, 0.26 m/s, 0.38 m/s, 0.46 m/s and 0.51 m/s).

For $U_{mf} = 0.065$ m/s, fixed hydrodynamic regime is established. Indeed, with a low superficial velocity, air flows simply through the particles, and no motion occurs, so the particle bed remains static. During the regime of minimal fluidization, at $U = 0.26$ m/s, the bed has been expanded, due to the ascending component of the air force counterbalancing the particles weight. Then the solid phase becomes suspended, and its volume fraction decreases from 0.63 to 0.57. At high superficial air velocities (0.38 m/s, 0.46 m/s, and 0.51 m/s), air bubble size increases and the bed expansion increases strongly, as illustrated in Fig. 8. This regime corresponds to the bubbling fluidization regime, glass beads volume fraction is important near sidewalls with a constant value around 0.58; glass beads particles have a tendency to concentrate on walls (dark red zone) rather than in reactor centre. Therefore, at large inlet air velocities, glass beads volume fraction distribution decreases in the middle of the bed, while air volume fraction increases. Similar outcomes have been observed by Sahoo and Sahoo (2014), for a hydrodynamic study of red mud particles of Geldart-A class. They found that by increasing the superficial gas velocities, small to large bubbles are formed and bed height extends, causing wall slug formation, manifested by high particles volume fraction near sidewalls. Whereas, Taghipour et al. (2005) explained that the growth in bubble size is driven by both sidewalls impacts and inter-bubble's interaction.

Figures 9 and 10 show snapshots of air and glass beads averaged axial velocity component over a time interval of 3-12s, for different inlet air velocities (0.065 m/s, 0.26 m/s, 0.38 m/s, 0.46 m/s and 0.51 m/s). At a low superficial

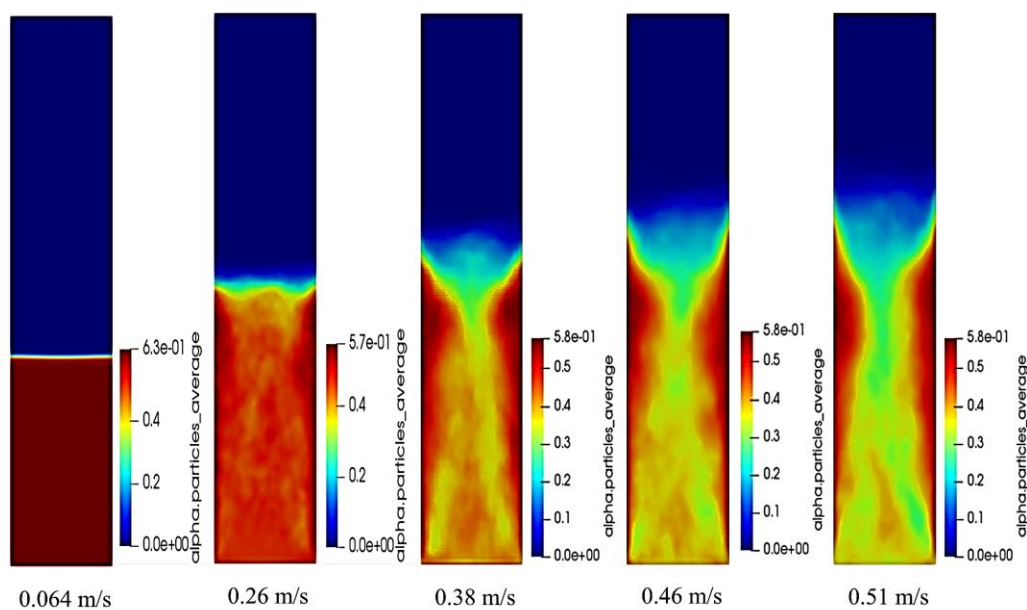


Fig.7. Influence of superficial air velocity on glass-beads volume fraction, over a time interval of (3-12s), and using Syamlal-O'Brien drag model.

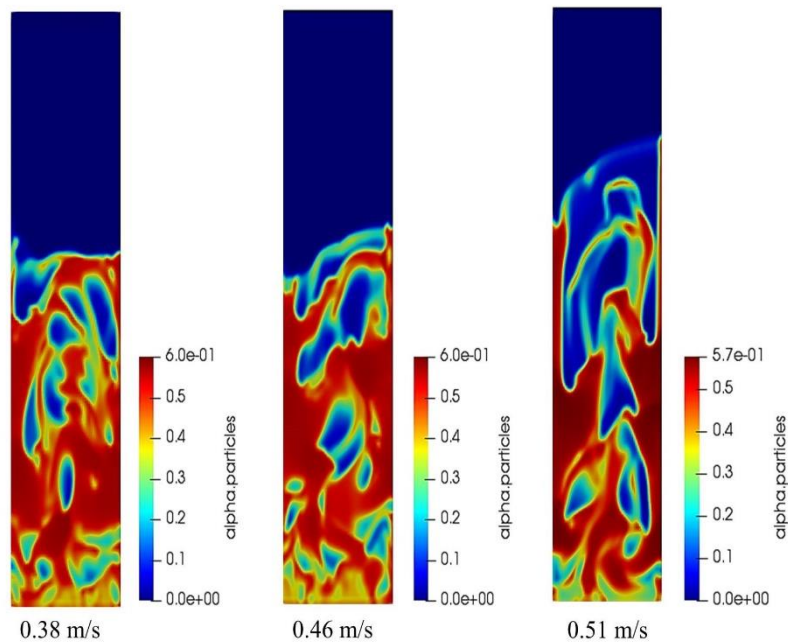


Fig. 8. Simulated glass-beads volume fraction profiles for high superficial air velocity of 0.38 m/s, 0.46 m/s and 0.51 m/s, using Syamlal-O’Brien drag model.

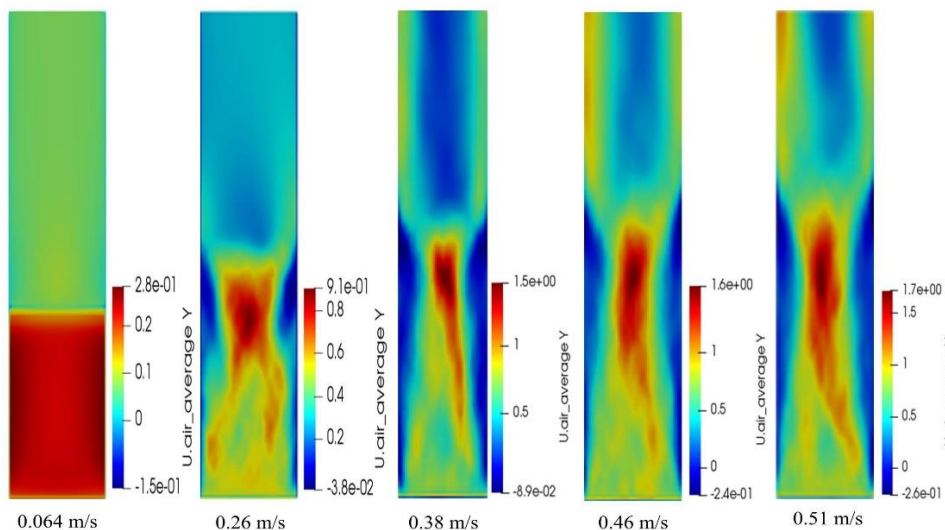


Fig. 9. Snapshots of averaged axial component of air velocity, over a time interval of 3-12s, and using Syamlal-O’Brien drag model.

air velocity $U = 0.065$ m/s, the air axial velocity distribution is homogeneous within bed and tends to become null at bed’s top. Moreover, particles bed is relatively fixed i.e., the solid phase velocity is low. With increasing inlet air velocity, air and glass beads axial velocities increase to 1.7 m/s and 0.65 m/s, respectively observed at $U = 0.51$ m/s. These velocities are important along the bed central region and smaller near sidewalls. In fact, at high superficial air velocities, large bubbles are formed in bed centre. Bubbles upward motion causes particles bed extension. It is manifested by the rise of the particles from the central region to the top, as well as, the deviation of a large fraction of solids towards reactor walls, which explains glass beads volume fraction distribution mentioned above.

5. CONCLUSION

In this paper, the attention was given to air-glass beads fluidized bed hydrodynamic aspect, by elaborating a numerical model based on two-phase Eulerian solver existing in OpenFoam v7. At first, Syamlal-O’Brien and Gidaspow models were used. Then, pressure loss, bed height expansion ratio, and air volume fraction distribution were calculated. After that, glass beads hydrodynamic aspect description was realized to analyse inlet air velocity influence on glass beads motion. Obtained results show the following major conclusions:

- Good consistency between experiment findings and computational predictions was observed,

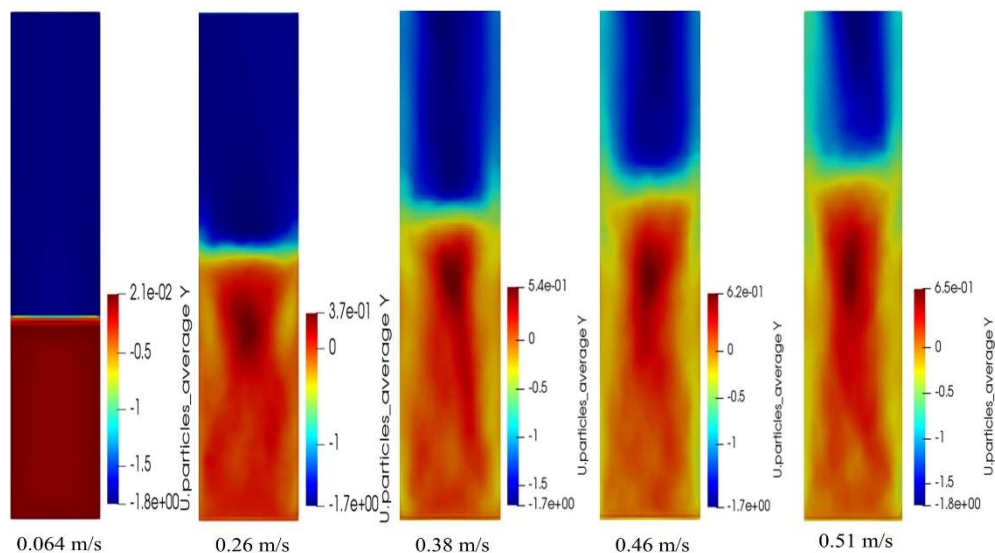


Fig. 10. Snapshots of averaged axial component of glass-beads velocity, over a time interval of 3-12s, and using Syamlal-O'Brien drag model.

proving accuracy of our numerical model developed on OpenFoam v7;

- Compared to other numerical results obtained by Ansys-Fluent and MFIX simulators, the results given by OpenFoam software show the lowest RMSE of 0.65 for pressure loss and 0.095 for bed expansion rate.
- Syamlal-O'Brien model give reliable predictions compared to Gidaspow model and was chosen to describe the hydrodynamic aspect.
- For low superficial air inlet ($U < U_{mf}$), no motion is detected until $U = 0.26$ m/s where the bed began expanding and glass beads volume fraction began to be slightly important near sidewalls.
- During bubbling regime ($U \geq U_{mf}$), air bubble size increases, glass beads volume fraction decreases in reactor centre, while air and glass beads axial velocities increase. These axial velocities are higher in reactor centre, and low in sidewalls, thus inducing the particles bed to expand strongly.

Finally, this study allowed us to have a clear insight of air-glass beads hydrodynamic behaviour in bubbling regime. Therefore, glass beads can be considered to be fluidizing fastly ($U_{mf} = 0.065$ m/s) which will be a good choice as an inert bed material for fluidized bed reactors to treat biomass. As futur perspectives, thermal and kinetic aspects will be added to the current model to assess energy recovery of municipal solid waste.

ACKNOWLEDGEMENTS

This study was performed within the framework of a research project funded by Ministry of National Education, Vocational Training, Higher Education and Scientific Research (Morocco) / Department of Higher Education and Scientific Research (MENFPESRS/DESRs). The authors would like to thank MENFPESRS/DESRs for the financial support.

CONFLICT OF INTEREST

The authors declare that they have no competing interests.

AUTHORS CONTRIBUTION

S. Aboudaoud: Conception and Design, data collection, results analysis, writing and editing the original draft. S. Touzani: Conceptualization, Supervision and Manuscript revision. S. Abderafi: Supervision, Manuscript revision and Project administration. A. Cheddadi: Supervision and Manuscript revision.

REFERENCES

- Aboudaoud, S., El Kourdi, S., Abderafi, S. & Abbassi, M. A. (2022). *Municipal solid waste generation from morocco and tunisia, and their possible energetic valorization*. 2021 9th International Renewable and Sustainable Energy Conference (IRSEC).
- Bhusare, V. H., Dhiman, M. K., Kalaga, D. V., Roy, S., & Joshi, J. B. (2017). CFD simulations of a bubble column with and without internals by using OpenFOAM. *Chemical Engineering Journal*, 317, 157–174. <https://doi.org/10.1016/j.cej.2017.01.128>
- Bounaceur, A. (2008). *Interaction lit fluidisé de particules solides-rayonnement solaire concentré pour la mise au point d'un procédé de chauffage de gaz à plus de 1000 K*. Phd thesis, École Nationale Supérieure des Mines de Paris, France. <https://pastel.archives-ouvertes.fr/tel-00409692>
- Cardoso, J., Silva, V., Eusébio, D., Brito, P., & Tarelho, L. (2018). Improved numerical approaches to predict hydrodynamics in a pilot-scale bubbling fluidized bed biomass reactor: A numerical study with experimental validation. *Energy Conversion and Management*, 156, 53–67. <https://doi.org/10.1016/j.enconman.2017.11.005>

- Chauhan, V., Chavan, P. D., Datta, S., Saha, S., Gajanan, S., & Dhaigu, N. D. (2022). A transient Eulerian-Eulerian simulation of bubbling regime hydrodynamics of coal ash particles in fluidized bed using different drag models. *Advanced Powder Technology*, 33(1), p. 103385. <https://doi.org/10.1016/j.appt.2021.12.004>
- Chen, M., Liu, M., & Tang, Y. (2019). Comparison of Euler-Euler and Euler-Lagrange Approaches for Simulating Gas-Solid Flows in a Multiple-Spouted Bed. *International Journal of Chemical Reactor Engineering*, 17(7). <https://doi.org/10.1515/ijcre-2018-0254>
- Fatti, V., & Fois, L. (2021). *CFD modeling of gas-solid fluidized beds in OpenFOAM: a comparison between the Eulerian-Eulerian and Eulerian-Lagrangian methods*. Master's Thesis, Politecnico di Milano. https://www.politesi.polimi.it/bitstream/10589/178957/3/2021_10_Fatti_Fois.pdf
- Di Renzo, A., Scala, F., & Heinrich, S. (2021). Recent Advances in Fluidized Bed Hydrodynamics and Transport Phenomena—Progress and Understanding. *Processes*, 9, 639. <https://doi.org/10.3390/pr9040639>
- Ding, J., & Gidaspow, D. (1990). A bubbling fluidization model using kinetic theory of granular flow. *AIChE Journal*, 36, 523–538. <https://doi.org/10.1002/aic.690360404>
- El Kourdi, S., Aboudaoud, S., Abderafi, S., & Cheddadi, A. (2022). Potential Assessment of Combustible Municipal Wastes in Morocco and their Ability to Produce Bio-Oil by Pyrolysis. *Materials Science Forum*, 1073, 149–154. Trans Tech Publications Ltd. <https://doi.org/10.4028/p-2gg5xu>
- El Kourdi, S., Aboudaoud, S., Abderafi, S., Cheddadi, A., & Ammar, A. M. (2023). Pyrolysis technology choice to produce bio-oil, from municipal solid waste, using multi-criteria decision-making methods. *Waste and Biomass Valorization*, 1-18. <https://doi.org/10.1007/s12649-023-02076-w>
- Gidaspow, D. (1994a). *Multiphase flow and fluidization*. San Diego: Academic Press, pp. 239-296. <https://www.sciencedirect.com/science/article/pii/B9780080512266500133>
- Gidaspow, D. (1994b). *Multiphase flow and fluidization: continuum and kinetic theory descriptions*. Academic Press.
- Herzog, N., Schreiber, M., Egbers, C., & Krautz, H. J. (2012). A comparative study of different CFD-codes for numerical simulation of gas–solid fluidized bed hydrodynamics. *Computers & Chemical Engineering*, 39, 41–46. <https://doi.org/10.1016/j.compchemeng.2011.12.002>
- Johnson, P. C., & Jackson, R. (1987). Frictional–collisional constitutive relations for granular materials, with application to plane shearing. *Journal of Fluid Mechanics*, 176, 67. <https://doi.org/10.1017/S0022112087000570>
- Kia, S. A., & Aminian, J. (2017). Hydrodynamic modeling strategy for dense to dilute gas–solid fluidized beds. *Particuology*, 31, 105–116. <https://doi.org/10.1016/j.partic.2016.06.004>
- Liu, Y., & Hinrichsen, O. (2014). CFD modeling of bubbling fluidized beds using OpenFOAM®: Model validation and comparison of TVD differencing schemes. *Computers & Chemical Engineering*, 69, 75–88. <https://doi.org/10.1016/j.compchemeng.2014.07.002>
- Lun, C. K. K., Savage, S. B., Jeffrey, D. J., & Chepuriniy, N. (1984). Kinetic theories for granular flow: inelastic particles in Couette flow and slightly inelastic particles in a general flow field. *Journal of Fluid Mechanics*, 140, 223–256. <https://doi.org/10.1017/S0022112084000586>
- Materazzi, M., & Lettieri, P. (2017). *Fluidized beds for the thermochemical processing of waste. Reference module in chemistry, molecular sciences and chemical engineering*. Elsevier. <https://doi.org/10.1016/B978-0-12-409547-2.12180-8>
- Ngo, S. I., Lim, Y. I., Song, B. H., Lee, U. D., Yang, C. W., Choi, Y. T., & Song, J. H. (2013). Hydrodynamics of cold-rig biomass gasifier using semi-dual fluidized-bed. *Powder Technology*, 234, 97–106. <https://doi.org/10.1016/j.powtec.2012.09.022>
- Pei, P., Zhang, K., & Wen, D. (2012). Comparative analysis of CFD models for jetting fluidized beds: The effect of inter-phase drag force. *Powder Technology*, 221, 114–122. <https://doi.org/10.1016/j.powtec.2011.12.043>
- Philippesen, C. G., Vilela, A. C. F., & Zen, L. D. (2015). Fluidized bed modeling applied to the analysis of processes: review and state of the art. *Journal of Materials Research and Technology*, 4, 208–216. <https://doi.org/10.1016/j.jmrt.2014.10.018>
- Sahoo, P., & Sahoo, A. (2014). Hydrodynamic studies on fluidization of Red mud: CFD simulation. *Advanced Powder Technology*, 25, 1699–1708. <https://doi.org/10.1016/j.appt.2014.06.017>
- Santos, D. A., Petri, I. J., Duarte, C. R., & Barrozo, M. A. S. (2013). Experimental and CFD study of the hydrodynamic behavior in a rotating drum. *Powder Technology*, 250, 52–62. <https://doi.org/10.1016/j.powtec.2013.10.003>
- Schaeffer, D. G. (1987). Instability in the evolution equations describing incompressible granular flow. *Journal of differential Equations*, 66(1), 19-50. [https://doi.org/10.1016/0022-0396\(87\)90038-6](https://doi.org/10.1016/0022-0396(87)90038-6)
- Shi, H., Komrakova, A., & Nikrityuk, P. (2019). Fluidized beds modeling: Validation of 2D and 3D simulations against experiments. *Powder Technology*, 343, 479–494. <https://doi.org/10.1016/j.powtec.2018.11.043>
- Solli, K. A., & Agu, C. (2017, September 25-27). Evaluation of Drag Models for CFD Simulation of

Fluidized Bed Biomass Gasification. The 58th Conference on Simulation and Modelling (SIMS 58) Reykjavik, Iceland. pp. 97-107. <https://doi.org/10.3384/ecp1713897>

Stanly, R., Shoen, G., & Kokhanchik, A. (2017). *Numerical simulation of gas-solid flows in fluidized bed with TFM model*. AIP Conference Proceedings, 1893(1). <https://doi.org/10.1063/1.5007498>

Syamlal, M., & Thomas, J. O. (1989). Computer simulation of bubbles in a fluidized bed. In *Fluidization and Fluid Particle Systems: Fundamentals and Applications* (Ed.) L. S. Fan, AIChE Symposium Series No. 270, 85, 22-31. <https://www.researchgate.net/publication/279892631>

Syamlal, M., Rogers, W., & O'Brien, T. J. (1993). *MFIX documentation: Volume 1, theory guide*. National Technical Information Service, Springfield, VA. <https://doi.org/10.2172/10145548>

Taghipour, F., Ellis, N., & Wong, C. (2005). Experimental and computational study of gas-solid fluidized bed hydrodynamics. *Chemical Engineering Science*, 60, 6857-6867. <https://doi.org/10.1016/j.ces.2005.05.044>

Ullah, A., Hong, K., Gao, Y., Gungor, A., & Zaman, M. (2019). An overview of Eulerian CFD modeling and simulation of non-spherical biomass particles. *Renewable Energy*, 141, 1054-1066. <https://doi.org/10.1016/j.renene.2019.04.074>

Ullah, A., Wang, W., & Li, J. (2013). Evaluation of drag models for cocurrent and countercurrent gas-solid flows. *Chemical Engineering Science*, 92, 89-104. <https://doi.org/10.1016/j.ces.2013.01.019>

Venier, C. M., Reyes Urrutia, A., Capossio, J. P., Baeyens J., & Mazza, G. (2019). Comparing ANSYS Fluent® and OpenFOAM® simulations of Geldart A, B and D bubbling fluidized bed hydrodynamics. *International Journal of Numerical Methods for Heat & Fluid Flow*, 30, 93-118. <https://doi.org/10.1108/HFF-04-2019-0298>

Yates, J. G., & Lettieri, P. (2016). *Fluidized-Bed Reactors: Processes and Operating Conditions*. Particle Technology Series, Cham: Springer International Publishing. <https://doi.org/10.1007/978-3-319-39593-7>

APPENDIX

Table A1. Equations calculating the different terms of the momentum conservation equations and the constitutive equations

Momentum Exchange Coefficients β_{g-s}

For coupling the gas-solid momentum exchange, the drag force model represented by the momentum exchange coefficient β_{g-s} is needed. It is calculated by the two following models:

- Syamlal-O'Brien model (Syamlal et al., 1993):

$$\beta_{g-s} = \frac{3}{4} \cdot \frac{\alpha_g \cdot \alpha_s \cdot \rho_g}{d_s \cdot v_{r,s}^2} \cdot C_D \cdot \frac{R_{es}}{v_{r,s}} \cdot |\bar{U}_s - \bar{U}_g| \quad (A1)$$

C_D is the drag coefficient representing the viscous force exerted into the particle and the dynamic pressure induced by fluid flow ratio:

$$C_D = \left[0.63 + 4.8 \left(\frac{R_{es}}{v_{r,s}} \right)^{-0.5} \right]^2$$

$$R_{es} = \frac{\rho_g \cdot d_s \cdot |\bar{U}_s - \bar{U}_g|}{\mu_g}$$

Reynolds number is given by:

Where, d_s and μ_g are the mean particle diameter and gas viscosity, respectively.

Particle terminal velocity correlation is given by:

$$v_{r,s} = 0.5(A - 0.06R_{es} + [(0.6R_{es})^2 + 0.12R_{es} \cdot (2B - A) + A^2]^{0.5})$$

With:

$$A = \alpha_g^{4.14}, B = 0.8\alpha_g^{1.28}, \text{ for } \alpha_g \leq 0.85$$

and $A = \alpha_g^{4.14}, B = \alpha_g^{2.65}, \text{ for } \alpha_g > 0.85$

- Gidaspow drag model (Gidaspow 1994a):

$$\beta_{g-s} = 150 \frac{\alpha_s^2 \cdot \mu_g}{\alpha_g \cdot d_s^2} + 1.75 \frac{\alpha_s \cdot \rho_g}{d_s} \cdot |\bar{U}_s - \bar{U}_g|, \quad \text{for } \alpha_g \leq 0.8$$

$$\beta_{g-s} = \frac{3}{4} \cdot \frac{\alpha_s \cdot \rho_g}{d_s} \cdot |\bar{U}_s - \bar{U}_g| \cdot C_D \cdot \alpha_g^{-3.65}, \quad \text{for } \alpha_g > 0.85 \quad (A2)$$

The Drag coefficient is given by:

$$C_D = \frac{24}{R_{es}} \left[1 + 0.15R_{es}^{0.687} \right], \text{ for } R_{es} < 1000$$

$$C_D = 0.44, \text{ for } R_{es} > 1000$$

Viscous Stress Tensors

For viscous fluid, the viscous stresses originated from frictions between the fluid and the surface of an element, is defined for the gas phase as:

$$\bar{\tau}_g = \mu_g \cdot [\nabla \bar{U}_g + \nabla^T \bar{U}_g] - \frac{2}{3} \mu_g \cdot (\nabla \bar{U}_g) \cdot \bar{I} \quad (A3)$$

For solid phase, the particles stress tensor incorporates shear viscosity, μ_s and bulk viscosity, λ_s , coming from solids momentum exchange due to translation and collision:

$$\bar{\tau}_s = (-p_s + \lambda_s \cdot \nabla \bar{U}_s) \bar{I} + \mu_s \cdot [(\nabla \bar{U}_s + (\nabla \bar{U}_s)^T) - \frac{2}{3} (\nabla \bar{U}_s)^T] \quad (A4)$$

Where \bar{I} is unit tensor.

Constitutive Equation

- Solid shear viscosity, μ_s measures the particle's resistance to flow. It includes three viscosity contributions: Collisional, Kinetic and frictional viscosities:

$$\mu_s = \mu_{s,col} + \mu_{s,kin} + \mu_{s,fr} \quad (A5)$$

Particle collisional viscosity, $\mu_{s,col}$ is related to particle collisions, which are considered as inelastic thanks to the use of the restitution coefficient e_{ss} , whose value is equal to 1 in case of perfectly elastic collisions and equal to 0 for completely inelastic collisions (Gidaspow 1994b):

$$\mu_{s,col} = \frac{4}{5} \alpha_s \cdot \rho_s \cdot d_s \cdot (1 + e_{ss}) \cdot g_{0,ss} \cdot \sqrt{\frac{\Theta_s}{\pi}} \quad (A6)$$

The solid kinetic viscosity, $\mu_{s,kin}$ is related to particle translation (Syamlal & Thomas, 1989) :

$$\mu_{s,kin} = \frac{\alpha_s \cdot \rho_s \cdot d_s \cdot \sqrt{\Theta_s \cdot \pi}}{6(3 - e_{ss})} \cdot [1 + \frac{2}{5}(1 + e_{ss}) \cdot (3e_{ss} - 1) \cdot g_{0,ss} \cdot \alpha_s] \quad (A7)$$

For Gidaspow (1994a) :

$$\mu_{s,kin} = \frac{10 \rho_s \cdot d_s \cdot \sqrt{\Theta_s \cdot \pi}}{96 \alpha_s (1 + e_{ss}) \cdot g_{0,ss}} \cdot [1 + \frac{4}{5}(1 + e_{ss}) \cdot g_{0,ss} \cdot \alpha_s]^2 \quad (A8)$$

Solid frictional viscosity, $\mu_{s,fr}$ accounts viscous-plastic conversion produced, once maximum particles volume fraction is reached (Schaeffer 1987):

$$\mu_{s,fr} = \frac{p_{s,fr} \sin \varphi}{2 \sqrt{I_{2D}}} \quad (A9)$$

Where, φ , I_{2D} , and $p_{s,fr}$ are internal friction angle, deviatoric stress tensor invariant and frictional pressure defined according to the Johnson and Jackson model by:

$$p_{s,fr} = F_r \cdot \frac{(\alpha_s - \alpha_{s,min})^2}{(\alpha_{s,max} - \alpha_{s,min})^5} \quad (A10)$$

Where: $Fr=0.05$

- Solid apparent viscosity, λ_s takes into account the solids resistance against compression and expansion (Lun et al., 1984):

$$\lambda_s = \frac{4}{3} \alpha_s^2 \cdot \rho_s \cdot d_s \cdot g_{0,ss} \cdot (1 + e_{ss}) \cdot \sqrt{\frac{\Theta_s}{\pi}} \quad (A11)$$

- Solids pressure, p_s appears in the solid phase momentum equation as pressure gradient term, ∇p_s . It is composed of two terms, one is kinetic and the other is related to solids collisions (Lun et al., 1984):

$$p_s = \alpha_s \cdot \rho_s \cdot \Theta_s + 2 \rho_s \cdot (1 + e_{ss}) \cdot \alpha_s^2 \cdot g_{0,ss} \cdot \Theta_s \quad (A12)$$

- Radial distribution function $g_{0,ss}$ express inter-grains collisions probability correction factor, applied for dense granular phase (Ding & Gidaspow, 1990). It is defined in Sinclair Jackson's model as:

$$g_{0,ss} = \left[1 - \left(\frac{\alpha_s}{\alpha_{s,max}} \right) \frac{1}{3} \right]^{-1} \quad (A13)$$

- Granular energy conductivity, κ_s (Syamlal & Thomas, 1989):

$$\kappa_s = \frac{15}{4(41 - 33\eta)} \cdot d_s \cdot \rho_s \cdot \alpha_s \cdot \sqrt{\pi \cdot \Theta_s} \cdot [1 + \frac{6}{5} \alpha_s \cdot g_{0,ss} \cdot (1 + e_{ss})]^2 + 2 \rho_s \cdot d_s \cdot \alpha_s^2 \cdot g_{0,ss} \cdot (1 + e_{ss}) \cdot \sqrt{\frac{\Theta_s}{\pi}} \quad (A14)$$

Following Gidaspow (1994a):

$$\kappa_s = \frac{150}{384(1 + e_{ss}) \cdot g_{0,ss}} \cdot d_s \cdot \rho_s \cdot \alpha_s \cdot \sqrt{\pi \cdot \Theta_s} \cdot [1 + \frac{12}{5} \eta^2 \cdot (4\eta - 3) \cdot \alpha_s \cdot g_{0,ss} + \frac{16}{15\pi} \cdot (41 - 33\eta) \cdot \eta \cdot \alpha_s \cdot g_{0,ss}] \quad (A15)$$

- Collisional energy dissipation, γ_s measures energy dissipated ratio caused by inter-particle inelastic collisions (Lun et al., 1984):

$$\gamma_s = \frac{12}{d_s \cdot \sqrt{\pi}} (1 - e_{ss}^2) \cdot \alpha_s \cdot \rho_s \cdot g_{0,ss} \cdot \Theta_s^{3/2} \quad (A16)$$